Probing Elementary Dislocation Mechanisms of Local Plastic Deformation by the Advanced Acoustic Emission Technique

A. Vinogradov[1], A. V. Danyuk[2], D. L. Merson[2] and I.S. Yasnikov[2]
[1] Department of Mechanical and Industrial Engineering, Norwegian University of Science and Technology – NTNU, Trondheim, N-7491, Norway
[2] Institute of Advanced Technologies, Togliatti State University, Togliatti, 445020, Russia

To gain a deeper insight into fundamental processes of localised plastic deformation, we propose a new strategy for micro-mechanical testing combining the micro-scale scratching and analysis of low amplitude acoustic emissions (AE) accompanying dynamic dislocation processes in solids. The analysis of the AE spectral density reveals its strong dependence on crystallographic orientations of the grains along the indenter path, thus reflecting the finest features of the local dislocation activity. Adding a temporal dimension with a sub-microsecond resolution, the proposed methodology substantially enhances the existing capacity of micro-mechanical testing and can be used in a wide range of testing schemes.

Keywords: deformation mechanisms; acoustic emission; microscopy; micro-mechanical testing.

Recently, a family of advanced micro-mechanical testing methods [1] emerged as significant tools for characterising the elastic-plastic mechanical response of materials on small scales. Providing an excellent reproducibility and accuracy of mechanical data, the instrumented indentation and scratch testing has become the primary technique to examine the local properties and to investigate the underlying local deformation and fracture mechanisms for a wide range of materials. A dislocation behaviour on the micro-scale is commonly characterised by the posttest analysis of slip patterns arising near the indenter footprint, while the local materials response is assessed by the load-displacement diagram or the coefficient of friction evaluated during a scratch test. However, the temporal resolution of these measurements is insufficient to reveal the details of the underlying dislocation dynamics. Real-time information on the elementary processes of local plastic deformation and fracture can substantially advance the capability of micro-mechanical testing. Providing this information with an unprecedented temporal resolution, the modern acoustic emission (AE) technique becomes increasingly recognised in micro-testing, e.g. during indentation [2] or scratch testing of ductile, brittle [3] and coated materials [4, 5]. The main challenge for the AE technique is to assess a very low amplitude signal generated in small, micrometres scale, deforming volumes. Because of the extremely low signal-to-noise ratio (SNR), the amplitude threshold-based methods fail to detect a signal from indentation or scratch testing of ductile materials. Another challenge arises when a link is sought between low amplitude AE signals and elementary deformation processes. To address these issues we have developed a versatile threshold-less AE signal recording and analysing procedure and applied it to the instrumented micro-scratching of copper polycrystals with the well-characterised initial microstructure.

The samples of 3N polycrystalline copper with dimensions of 20×20×2mm^3 were annealed in vacuum at 1170K for 1 h and electrolytically polished to a mirror-like finish. The microstructure was investigated by electron backscattered diffraction (EBSD) measurements in a field-emission scanning electron microscope (SEM) ZEISS-SIGMA equipped with the EDAX/TSL EBSD detector. Scratch tests were carried out using the Nanovea tester. To reduce the effect of interfacial friction between stylus and specimen [6-8], the Berkovich diamond indenter in the edge-forward orientation was moved linearly at relatively high constant dragging speed V_S =12 and 24mm/min until the scratch reaches 2 mm length. The normal load F during the test was set constant at the minimum stable controllable value 1N. The piezoelectric sensor AE-900S-WB (NF-Electronics, Japan) with a frequency band of 100-1000kHz was attached to the samples through vacuum oil with a rubber band. The signals were amplified by 60dB by the low-noise pre-amplifier and acquired by the 16-bit PCI-2 board (MISTRAS, USA) operated in a continuous threshold-less mode at the sampling rate of 5MSamples/s.

During signal processing (i) the continuously streamed data were sectioned into consecutive individual realisations of 8192 readings; (ii) a power spectral density (PSD) function $G(f)$ was calculated using a Welch technique; (iii) the average (per realisation) *power* $P_{AE} = \int_{f_{\min}}^{f_{\max}} G(f)\,df$, and the *median frequency* f_{m} of the PSD function defined by the implicit equation $\int_{f_{\min}}^{f_{\mathrm{m}}} G(f)\,df = \int_{f_{\mathrm{m}}}^{f_{\max}} G(f)\,df$ were introduced (see [9] for details); (iv) the time-series of these variables were further smoothed by low-pass Butterworth filtering with the cut-off frequency of 19 Hz. Both P_{AE} and f_{m} were obtained from *G(f)* after subtraction of the mean PSD of the laboratory noise pre-recorded before the start of loading during each test.

The specimen grain structure revealed by the EBSD technique is shown in Fig.1a in the inverse pole figures (IPF) colours with the superimposed view of the scratch. The rigid stylus moved along several grains with different orientations. As the size of the indenter footprint is usually smaller than the grain size, one can consider that the indenter ploughs a micro-groove in single crystals separated by grain boundaries. Slip systems with the largest Schmid factor are activated under indenter in each grain. The crystallographic elastic and plastic anisotropy of the grains causes a direction dependent variation in the dislocation behaviour. Near the grain boundaries, the morphology of the scratch has visible facets signifying changes in the materials resistance to the indenter motion due to the interaction between the boundary and the lattice dislocations generated in the plastic zone ahead of the indenter as illustrated in Fig.1c.

A typical example of the recorded raw AE signal is shown in Fig.1b. AE is a transient phenomenon resulting from a rapid stress drop in a local region of the deforming solid [10]. Nonetheless, the AE waveform during scratch testing appears as a continuous noise-like signal with a very low amplitude, cf. Fig.1b, which is typically observed during uniform plastic deformation mediated by dislocations in pure metals [11]. No microcracks were observed by SEM within the scratch imprint. It is, therefore, plausible to suppose that the primary source of AE is associated with plastic deformation. The SNR of the signal shown in Fig.1 is far too low to enable any conventional threshold-based AE analysis, which is commonly used for detection of transient signals. However, considering the stationarity of the recorded AE stream

in a wide sense, the Fourier spectral representation provides a convenient means to characterise the signal and to reveal its fine features depending on the dislocation activity in differently oriented grains. Using an original signal categorization technique (see Supplementary Material on-line), it was demonstrated that the AE signal generated throughout scratching is uniform, i.e. it is produced by the sources belonging to the same parent population. Figures 2 show the behaviour of the AE spectral parameters P_{AE} and f_m during scratch testing with different velocities. One can notice that a combination of these variables reflects the changes in the grain microstructure along the scratch path. When the indenter crosses a grain boundary, new slip systems are activated resulting in the change of the hardening rate controlled by the dislocation storage rate in different slip systems. The AE behaviour changes accordingly, although these changes are not necessarily very sharp since the dimensions of the indenter are much greater that the grain boundary thickness.

A strong AE dependence on the crystallographic orientation of single crystals tested in tension has been convincingly demonstrated in many early studies [12, 13]. Particularly, the relation exists between the AE parameters - P_{AE} and f_m - and the strain hardening rate resulting from activation of different slip systems in differently oriented crystals [9, 11, 14]. Despite the very low SNR and the fluctuating behaviour of P_{AE} and f_m in Figs.2a,b, the strong AE dependence on the crystallographic orientation of the grains under the indenter is particularly evident on the scatter-plot P_{AE} vs. f_m, Figs.2c,d. The parameters characterising AE from different grains form compact clusters, Figs.2a,b, with remarkably different centroids (f_m,P_{AE}). Their positions and shapes depend on the crystallographic orientation of the grain, i.e. on the specific dislocation behaviour and hardening in different grains. The green circles "connecting" the dense clusters in Figs.2c,d are not indexed as independent clusters. Rather, they represent reasonably the transition AE behaviour of the indenter passing through the grain boundary. It is important to notice that the average P_{AE} value increased by a factor of two from 0.015 to 0.03a.u. with the twofold increase in V_S . It is important to notice here that the scratching velocity exerts opposite effects on adhesive friction and AE: interfacial friction reduces [15, 16] while AE increases with the increasing velocity. The observed behaviour corroborates the assumption that the effect of plastic deformation overrides the possible effect of interfacial friction. On the other hand, the proportionality between the AE power and plastic strain rate has long been recognised as the essential feature of continuous AE accompanying plastic deformation of metals [17]. Taking into account that the mean hardness did not change appreciably between these two tests and that for the scratching test the shear strain rate is defined as $\dot{\gamma} = V_S / W_S$ (with W_S -the width of the scratch) [18], one can conclude that the same proportionality holds in scratch testing. It is also good to notice that $\dot{\gamma}$ during scratching is usually much higher than in conventional tensile tests (e.g. $\dot{\gamma} = 2.5\ s^{-1}$ and $\dot{\gamma} = 5 s^{-1}$ for V_S =12 and 24mm/min, respectively).

Dislocations emerging at a free surface are known as powerful AE sources [19]. Fine slip lines are clearly visible in the plastic zone ahead of the indenter tip, Fig.1c. The plastic zone has been considered approximately semi-spherical with the radius of $1.5 \div 2.2 W_S$ [8, 20]. The plastic zone can be visualised as illustrated in Fig.1c: the white circle indicates approximately the area where the "strongest" AE sources – i.e. dislocations escaping to the free surface in an

undeformed part of the crystal – are located. As the stylus drags along the crystal surface, a fresh part of the material is persistently exposed to local loading ahead of the indenter. This ensures the stationarity and excellent reproducibility of the AE signal on average during scratch testing. A high density of slip lines is observed in the intimate vicinity to the scratch. In fact, such a heavily deformed material ceases to produce measurable AE because of strong hardening impeding dislocation motion. It has been well understood that the AE signal caused by dislocation motion is lower when the resistance to dislocation slip is higher [21]. That is why the AE signal peaks sharply around the yield point in pure metals. It then reduces quickly as hardening proceeds [9, 22]. The interaction of mobile dislocations with immobile ones reduces the dislocation free path and thus hinders the dislocation mobility when strain increases. Thus, one can reasonably assume that the measured AE signal is associated primarily with dislocation escaping to the free surface ahead of the stylus.

The scratch hardness H_S of single crystal copper is anisotropic and dependent on the crystallographic direction. The H_S value is connected to the plastic flow through the scaling relation $H_S \sim \tau \sim \sqrt{\rho}$ [15, 23], resembling the familiar Taylor relation between the dislocation density ρ and the shear flow stress τ in crystals. After passing the grain boundary, the indenter penetrates into an undeformed grain where H_S changes according to the dislocation behaviour controlled by the crystallographic orientation of the grain. Therefore, the AE behaviour should be correlated with the scratch hardness. In the first order approximation, let us consider a single dislocation moving on a slip plane near the free surface under the action of the image force F_{im} with the instantaneous velocity u. The applied force and other interactions between moving or static dislocations are neglected here, which is a reasonable approximation if one considers the slip occurring in the undeformed part of the crystal, Fig.1c. The attractive image force increases in inverse proportion to the distance *x* between the dislocation and the free surface. In equilibrium conditions, this force (per unit length of the dislocation *L*) can be derived in the glissile direction for different dislocation configurations [24] as:

$$\frac{F_{im}}{L} = \frac{Gb^2}{4\pi x} \quad (for \quad screw); \quad \frac{F_{im}}{L} = \frac{Gb^2}{4\pi(1-\nu)x} \quad (for \quad edge) \tag{1}$$

where *b* is the magnitude of the Burgers vector, *G* is the shear modulus, and ν is the Poisson ratio. The AE power p_{AE} associated with the energy dissipated per unit time during the motion of a single dislocation segment can be phenomenologically expressed as

$$\frac{p_{AE}}{L} \sim \frac{F_{im}}{L} u \tag{2}$$

The instantaneous dislocation velocity u during the free flight differs from the average velocity $\langle V \rangle$ which is controlled by the waiting time at the obstacles and which enters the Orowan equation for the shear strain rate $\dot{\gamma} = \rho_m b \langle V \rangle$ with ρ_m denoting the density of mobile dislocations. The resultant AE signal such as that shown in Fig.1b is produced in the crystals by multiple dislocation segments moving towards the free surface, escaping there and

forming the step-wise slip lines. The measured AE power P_{AE} is found as a product of the normalised AE power p_{AE}/L and the total length of mobile dislocations L_m in the effective volume V_{pl} where plastic deformation occurs ahead of the indenter:

$$P_{AE} = \frac{p_{AE}}{L} L_m = \frac{p_{AE}}{L} \rho_m V_{pl} \sim \frac{Gb^2 u}{4\pi\delta} \rho_m V_{pl} \tag{3}$$

where δ is a constant characterising the image-force-induced surface effect on the dislocation distribution [25, 26] and the dislocation depleted zone thickness. The median frequency of the AE power spectral density is determined by the dislocation relaxation time and can be expressed by the ratio of the average dislocation velocity and the mean free path $\langle \Lambda \rangle$: $f_m = \langle V \rangle / \langle \Lambda \rangle$ [11] (for comparison with experiments, this quantity should be corrected for the sensor response and the transfer function [11]). To avoid the obvious uncertainty associated with unknown ρ_m and $\langle V \rangle$ it is convenient to combine the last expression with Eq.(3). Then, using the Orowan equation and taking $V_{pl} \sim \langle \Lambda \rangle^3$ we obtain

$$P_{AE} f_m \sim \frac{Gb^2 u}{4\pi\delta} \rho_m V_{pl} \frac{\langle V \rangle}{\langle \Lambda \rangle} \sim \frac{Gbu\dot{\gamma} \langle \Lambda \rangle^2}{4\pi\delta} \tag{4}$$

Considering that dislocations near the free surface move fast [27] (at a large fraction of the velocity of sound) in the rapidly increasing field of the image force, one can plausibly assume that dislocations in the high-speed regime move with the velocity linearly proportional to the resolved shear stress τ: $\tau b = Bu$, where B is the temperature dependent drag coefficient [28]. Considering that $\langle \Lambda \rangle$ scales with $1/\tau$, Eq.(4) reduces to

$$P_{AE} f_m \sim \frac{Gb^2 \tau \dot{\gamma}}{4\pi B\delta} \langle \Lambda \rangle^2 \sim \frac{\dot{\gamma}}{\tau} \sim \frac{V_S}{\sqrt{H_S}} \tag{5}$$

where the scratch hardness was evaluated according to the ASTM G171-03 standard [29], as $H_S = 24.98 \frac{F}{W_S^2}$ where 24.98 is the geometrical constant and W_S measured directly from the residual scratch impression; the proportionality between τ and H_S holds due to the familiar Schmid-Boas equation [23, 30]. The latter expression predicting the inverse relation between $P_{AE} f_m$ and $\sqrt{H_S}$ allows for simple verification and appears in fair agreement with experiment as shown in Fig.3 for both tests performed with different scratch velocities. Each point on this graph is represented by the centroid of the corresponding cluster, from Figs.2c,d, and the error bars are calculated as the standard deviations of $P_{AE} f_m$ products in each grain. The scatter observed in this plot is likely associated with the orientation dependence of the strain rate entering Eq.(5), which is neglected in the present simplistic model and which will be included in a more elaborate formulation by accounting for the distribution of resolved shear stresses as a function of sliding direction through the modified Schmid-Boas approach. Importantly is that the slopes of the obtained regression lines for the tests performed with

different stylus velocities are different by approximately a factor of two (within the experimental scatter) as predicted by Eq.(5). Thus, despite the simplicity, the model provides a reasonable first-order explanation to the observed results.

In conclusion, micro-mechanical testing offers distinct advantages over conventional macroscopic techniques for characterisation of fundamental processes governing plastic flow in small volumes. The proposed processing of AE arising under local load provides additional information (which is inaccessible otherwise) on details of the dislocation behaviour depending on the local grain crystallography. The proposed methodology is by no means specific to scratch testing and can be easily adapted to other micro-mechanical testing schemes. In the forthcoming publication, we endeavour to demonstrate that employing the same technique powered by an optimal "denoising" strategy enables revealing the transient nature of AE signals caused by individual slip lines and gaining a deeper insight into the intermittency of plastic flow.

Financial support from the State Assignment of the Ministry of Science and Education of Russia according to the contract N 11.5281.2017/8.9 is gratefully appreciated.

References.

[1] M.D.Uchic, D.M.Dimiduk, R.Wheeler, P.A. Shade, H.L. Fraser, Scripta Materialia, 54 (2006) 759-764.
[2] N.H. Faisal, R. Ahmed, R.L. Reuben, International Materials Reviews, 56 (2011) 98-142.
[3] V. Perfilyev, I. Lapsker, A. Laikhtman, L. Rapoport, Tribology Letters, 65 (2017) 24.
[4] B. Podgornik, O. Wänstrand, Materials Characterization, 55 (2005) 173-178.
[5] E. Agletdinov, E. Pomponi, D. Merson, A. Vinogradov, Ultrasonics, 72 (2016) 89-94.
[6] J.A. Williams, Tribology International, 29 (1996) 675-694.
[7] H.R. Chamani, M.R. Ayatollahi, Tribol. Int., 103 (2016) 25-36.
[8] F. Wredenberg, P.L. Larsson, J Mech Mater Struct, 2 (2007) 573-594.
[9] A. Vinogradov, M. Nadtochiy, S. Hashimoto, S. Miura, Mater Trans JIM, 36 (1995) 496-503.
[10] C.B. Scruby, H.N.G. Wadley, J.J. Hill, Journal of Physics D, 16 (1983) 1069-1083.
[11] A. Vinogradov, I.S. Yasnikov, Y. Estrin, Journal of Applied Physics, 115 (2014) 233506
[12] Z.I. Bibik, Physics of Metals and Metallography, 59 (1985) 182-186.
[13] R.T. Sedgwick, Journal of Applied Physics, 39 (1968) 1728-1740.
[14] A. Vinogradov, M. Nadtochiy, S. Hashimoto, S. Miura, Mater Trans JIM, 36 (1995) 426-431.
[15] P.L. Menezes, M. Nosonovsky, S.V. Kailas, M.R. Lovell, Friction and Wear, in: P.L. Menezes, M. Nosonovsky, S.P. Ingole, S.V. Kailas, M.R. Lovell (Eds.) Tribology for Scientists and Engineers: From Basics to Advanced Concepts, Springer, New York, 2013, pp. 43-91.
[16] B.J. Briscoe, S.K. Biswas, S.K. Sinha, S.S. Panesar, Tribol Int, 26 (1993) 183-193.
[17] H. Hatano, Journal of Applied Physics, 47 (1976) 3873-3876.
[18] B.J. Briscoe, E. Pelillo, S.K. Sinha, Polymer Eng & Sci, 36 (1996) 2996-3005.
[19] D. Merson, M. Nadtochiy, V. Patlan, A. Vinogradov, K. Kitagawa, Mater Sci Eng A, 234 (1997) 587-590.
[20] K.L. Johnson, Contact mechanics, Cambridge University Press, Cambridge, 1987.
[21] K. Ono, J Acoust Soc Am, 64 (1978) S174-S175.
[22] C.R. Heiple, S.H. Carpenter, J. Acoustic Emission., 6 (1987) 177-237.
[23] X. Hou, N.M. Jennett, Acta Materialia, 60 (2012) 4128-4135.
[24] J.P. Hirth, J. Lothe, Theory of dislocations, 2nd ed., Wiley, New York, 1982.
[25] H. Mughrabi, physica status solidi (b), 44 (1971) 391-402.
[26] J.T. Fourie, The Philosophical Magazine A, 17 (1968) 735-756.
[27] H. Godon, H.H. Potthoff, H. Neuhäuser, Crystal Research and Technology, 19 (1984) 373-385.
[28] V.A. Al'shitz, V.L. Indenbom, Soviet Physics Uspekhi, 18 (1975) 1.
[29] ASTM G171-03 (2017) Standard Test Method for Scratch Hardness of Materials Using a Diamond Stylus, West Conshohocken, PA, 2017, https://doi.org/10.1520/G0171-03R17.
[30] C.A. Brookes, P. Green, Proc of the Royal Society of London: A, 368 (1979) 37-57.

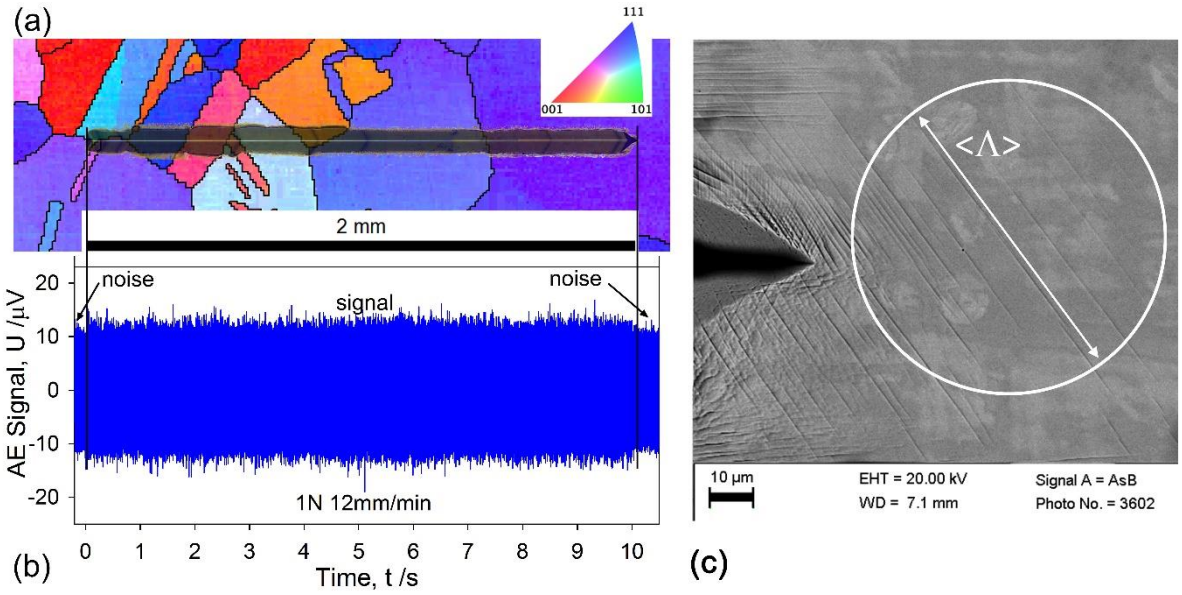

Figure 1. EBSD orientation map of the surface of pure Cu polycrystal with the superimposed optical microscopy image of the scratch (the map is coded in the invers pole figures colours corresponding to the standard triangle shown in the inset) (a); corresponding raw AE stream (b), vertical lines indicate the beginning and the end of the scratching process; backgound noise is seen before 0s and after 10s; SEM micrograph showing the dislocation slip pattern ahead of the indenter tip (c); the white circle indicates schematically the plastic zone where the active sources of AE are seen as individual slip lines in the primary slip system (other slip systems are visible in the severely deformed region in the proximity to the indenter tip).

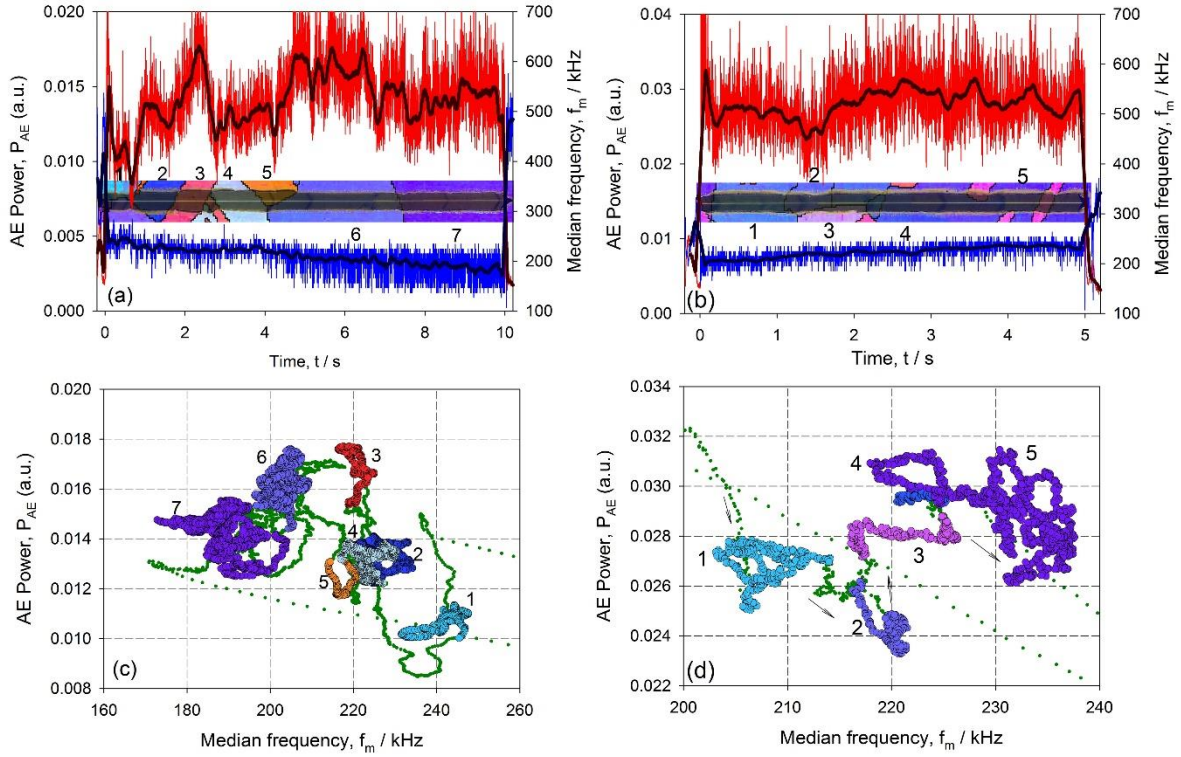

Figure 2. AE power (red online) and median frequency (blue online) as a function of scratching time for two test performed with different scratch velocities (a) V_S=12mm/min and (b) V_S=24mm/min. Images of the scratch path in the grain structure corresponding to the observed AE history are shown in the insets. Solid black lines represent low-pass smoothed data. Bi-variate P_{AE} vs. f_m distributions highlighting the AE patterns in different grains are shown (c) and (d). The grains along the scratch path are numerically labelled on the EBSD map and the corresponding P_{AE} vs. f_m clusters are inked accordingly.

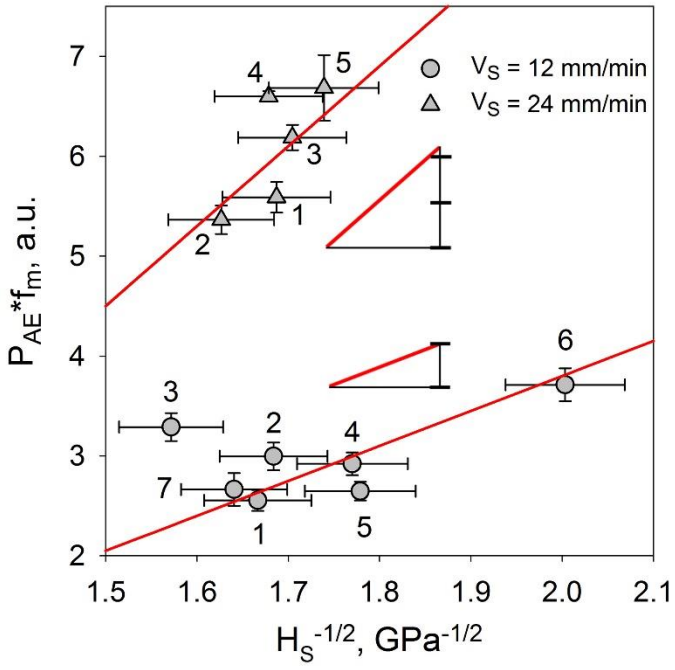

Figure 3. A linear regression (solid lines) showing the inverse relation between the $P_{AE} f_m$ product and $\sqrt{H_S}$ predicted by Eq.(7) for the two tests performed with different V_S. Each point on the graph corresponds to one grain passed by the indenter in Figs.2a and b (points are labelled by the same numbers as the grains in Fig.2). Notice that, in line with Eq.(7), the slope between the two lines differs approximately by a factor of two as also does the scratch velocity V_S .